Design of a two Phase Radio Frequency Drive for Ion Traps using a Lumped Elements Resonator

Arne Thomsen
athomsen@ethz.ch

July 2020

Supervisors:
Nick Schwegler
Dr. Daniel Kienzler
Prof. Dr. Jonathan Home

Institute for Quantum Electronics, ETH, 8093 Zurich, Switzerland

Contents

1 Introduction

One of the experiments currently in development in the trapped ion quantum information group at ETH Zürich aims at trapping Be^+ and H_2^+ ions to perform high precision spectroscopy on the molecule [1]. At the heart of the experiment, a linear Paul trap is used to confine the ions (see Fig. 1). To produce the radial trapping potential, four electrodes are connected to a voltage source oscillating at a radio frequency (RF). For reasons related to the ion confinement, the RF voltage at the diagonal rods are in phase, while the voltage at neighboring rods is shifted by 180° relative to each other. Therefore, the ion trap drive has to provide two voltages differing only in phase. They are denoted "RF+" and "RF-". The drive is chosen to be a resonant circuit because of the desirable voltage amplification and frequency filtering.

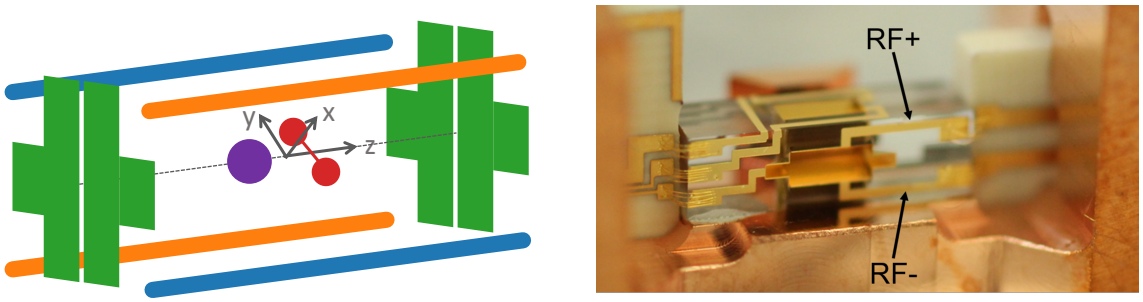

(a) Sketch of the trap. The four radially confining electrodes are illustrated in blue (RF+) and orange (RF-), the end caps in green. Along the trap axis z, a Be^+ ion (violet) and H_2^+ ion (red) are shown.

(b) Closeup photograph of the trap. The two trap electrodes visible from this angle are marked with arrows.

Figure 1: Linear Paul trap of the Molecule experiment.

The aim of this semester project is to design a resonant circuit drive using lumped elements. This report is divided into sections that follow the order of the consecutive considerations. Section 2 briefly outlines the theory behind ion trapping using electric RF fields and the series RLC circuit. Section 3 explains why a drive consisting of lumped elements and providing two out-of-phase RF signals is chosen for the experiment. Section 4 is concerned with the conception of the schematic and divided into the sub circuits that make up the full resonant circuit. Section 5 is about the design of the PCB and section 6 finally outlines the future steps that need to be taken to successfully incorporate the drive into the experiment.

2 Theory

2.1 Trapping of Ions using RF Electric Fields

This brief section follows chapter 2 in [2] and chapter 2.1 in [3]. To perform quantum information processing experiments on a system like an ion, it needs to be isolated from its surroundings and kept in place. This is achieved with a so called ion trap. There are two common ways in which charged particles like ions can be confined for this purpose. Penning traps, which employ static

electric and static magnetic fields. And Paul traps, where the confining potential is created using both static and oscillating electric fields. In the following, the focus lies on linear Paul traps.

For an ion to be trapped in three dimensions, it needs to experience a restoring force when it is displaced in any direction from the origin. The simplest potential fulfilling this criterion is harmonic and given by

$$\Phi(x, y, z) = \frac{1}{2} V(\alpha x^2 + \beta y^2 + \gamma z^2), \tag{1}$$

where the coefficients α, β and γ must all be strictly positive to result in a confining potential in that direction. Poisson's equation for a static electrical potential in three dimensional space reads

$$\nabla^2 \varphi = -\frac{\rho}{\varepsilon}, \tag{2}$$

where φ is a static eletrical potential, ρ the charge density and ε the dielectric constant. Plugging in equation (1) for free space $\rho = 0$ leads to the condition

$$\nabla^2 \Phi(x, y, z) = \alpha + \beta + \gamma = 0, \tag{3}$$

which shows that not all of the coefficients can be positive at the same time. A static potential therefore has to be anti confining in at least one spatial direction. The potential forms a saddle, not a minimum, hence it can not trap an ion.

The solution to this is using an electrical potential $\Phi(x, y, z, t)$ that oscillates at a radio frequency (RF) Ω_{RF}. For every moment in time the potential then still has the shape of a saddle, but the direction of this saddle oscillates with the radio frequency. The full ion trap potential including a static DC term looks like

$$\begin{aligned} \Phi(x, y, z, t) &= \Phi_{\mathrm{DC}}(x, y, z) + \Phi_{\mathrm{RF}}(x, y, z, t) && (4) \\ &= \frac{1}{2} V_{\mathrm{DC}} \left(\alpha_{\mathrm{DC}} x^2 + \beta_{\mathrm{DC}} y^2 + \gamma_{\mathrm{DC}} z^2 \right) && (5) \\ &+ \frac{1}{2} V_{\mathrm{RF}} \cos\left(\Omega_{\mathrm{RF}} t\right) \left(\alpha_{\mathrm{RF}} x^2 + \beta_{\mathrm{RF}} y^2 + \gamma_{\mathrm{RF}} z^2 \right) && (6) \end{aligned}$$

and also has to fulfill equation (2) at every single moment in time. Under the assumption that $\omega_m \ll \Omega_{\mathrm{RF}}$[1], the RF potential can be approximated as a time independent pseudopotential

$$\bar{\Phi}_{\mathrm{RF}}(\bar{x}, \bar{y}, \bar{z}) = \frac{q^2 V_{\mathrm{RF}}^2}{4 m \Omega_{\mathrm{RF}}^2} \left(\alpha_{\mathrm{RF}}^2 \bar{x}^2 + \beta_{\mathrm{RF}}^2 \bar{y}^2 + \gamma_{\mathrm{RF}}^2 \bar{z}^2 \right), \tag{7}$$

where m is the ion mass, q the ion charge and the ion movement is separated $x = \bar{x} + \chi$ into a slow and fast (micromotion) part. In a harmonic oscillator pseudopotential approximation, only the slowly varying change in position is taken into account. This potential is now confining in all spatial directions since the prefactors of the coordinates are strictly positive for non vanishing α_{RF}, β_{RF} and γ_{RF}.

[1] that is, the frequency of the ion's motion (see [2] for a derivation) is much smaller than the RF frequency with which the potential oscillates

2.2 Series RLC Circuit

The RF voltages of the ion trap (see previous section) are typically driven by an RF source connected to a resonant circuit. This is done for two main reasons: Firstly, the resonator amplifies the RF voltage. This is of concern since the needed RF voltage amplitude dictated by the specific trap geometry is typically larger than what can be produced by commercially available function generators. Secondly, a resonator circuit acts as a spectral filter and suppresses the voltage amplitude of off-resonant frequencies. This is desirable to operate the trap at a single radio frequency Ω_{RF} and suppress noise.

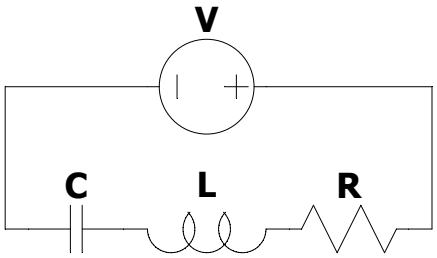

Figure 2: Schematic of a series RLC circuit.

A simple type of lumped element resonator is given by the series RLC circuit only consisting of a single resistor (R), inductor (L) and capacitor (C) (see Fig. 2). In the case considered in this report, the C is the capacitance of the ion trap and the finite R is attributed to the non vanishing resistance of the connecting wires and inductor coil.

During the oscillation, the energy stored in the circuit is converted back and forth from the electrical field (as a voltage across the capacitor) to the magnetic field (as a current through the inductor). Power is dissipated through the resistance, dampening this process.

The discussion below follows [3] where it is not stated otherwise. A distinction is made between an RLC circuit driven by a source with vanishing and non vanishing impedance Z_s.

2.2.1 Driven by an Ideal Source ($Z_s = 0\,\Omega$)

When there is an alternating voltage driving the circuit, it can be shown [4] that resonance occurs at the natural frequency

$$\omega_0 = \frac{1}{\sqrt{LC}}, \tag{8}$$

which is the same as the frequency at which a free undamped LC circuit oscillates. At ω_0, the voltage ratio $V_{\mathrm{out}}/V_{\mathrm{in}}$ is maximal and defines the so called voltage gain G_V as

$$G_V \overset{\mathrm{def}}{=} \frac{|V_{\mathrm{out}}^{\mathrm{max}}|}{|V_{\mathrm{in}}|} = \frac{1}{R}\sqrt{\frac{L}{C}} = \frac{\omega_0 L}{R}, \tag{9}$$

where V_{out} is measured at the capacitor and V_{in} at the source. For a generic resonator, the so called quality factor Q is defined as (see reference [5])

$$Q \overset{\mathrm{def}}{=} 2\pi \times \frac{\text{energy stored}}{\text{energy dissipated per cycle}}. \tag{10}$$

In the case of the series RLC with sinusoidally oscillating current $I = I_0 \sin(\omega_0 t)$, the energy stored in the circuit is equal to the energy stored inside the magnetic field when the current is maximal and consequently given by $W_{\text{stored}} = \frac{1}{2} L I_0^2$. The power dissipated during one full oscillation can be calculated as

$$P_{\text{dissipated}} = \int_0^T U(t) I(t) \, \mathrm{d}t = R \int_0^T I^2(t) \, \mathrm{d}t = R \int_0^{\frac{2\pi}{\omega_0}} I_0^2 \sin^2(\omega_0 t) \, \mathrm{d}t = \frac{\pi}{\omega_0} R I_0^2. \tag{11}$$

Plugging these results at into equation (10) finally yields the result

$$Q = 2\pi \frac{\frac{1}{2} L I_0^2}{\frac{\pi}{\omega_0} R I_0^2} = \frac{\omega_0 L}{R} = G_V. \tag{12}$$

Since every real inductor coil also has a parasitic capacitance and can therefore act as a resonating circuit by itself, the quality factor can also be expressed for a single inductor coil and is then equal to

$$Q_L(\omega) = \frac{\omega L}{R}. \tag{13}$$

A high quality factor, which is an often cited metric given by manufacturers, therefore corresponds to a low series resistance R.

It can also be observed that the circuit's impedance is purely real at resonance because the imaginary part of the total circuit's impedance equal to the sum of the inductor's (Z_L) and capacitor's (Z_C) impedance vanishes by definition of ω_0:

$$Z_L = i\omega_0 L = i\sqrt{\frac{L}{C}} = -\left(-\frac{i}{\omega_0 C}\right) = -Z_C. \tag{14}$$

2.2.2 Impedance Matched to Real Source ($Z_s \neq 0\,\Omega$)

A real life source has a certain impedance Z_s, which is typically equal to $50\,\Omega$. To prevent power from being reflected back to the source instead of being transferred to the load, the load's impedance Z_l has to fulfill

$$Z_l = Z_s^*. \tag{15}$$

This criterion is called impedance matching and can be realized in various ways of which two are briefly discussed in section 4.4. Impedance matching is essential to getting the desired maximal voltage gain at resonance.

The voltage gain G_V^m of an impedance matched series RLC circuit can be related to previously discussed quantities through the equalities [3]

$$G_V^{\text{m}} = \sqrt{\frac{L}{Z_s R C}} = \frac{\omega_0 L}{\sqrt{Z_s R}} = \sqrt{\frac{Q}{\omega_0 Z_s C}}. \tag{16}$$

3 Dual RF Resonator Preliminaries

This section introduces the concept of what is referred to as dual RF throughout this report. It is an alternative scheme to drive a Paul trap that relies on out of phase RF generation as opposed to a single RF drive where two electrodes are grounded.

3.1 Dual RF Motivation

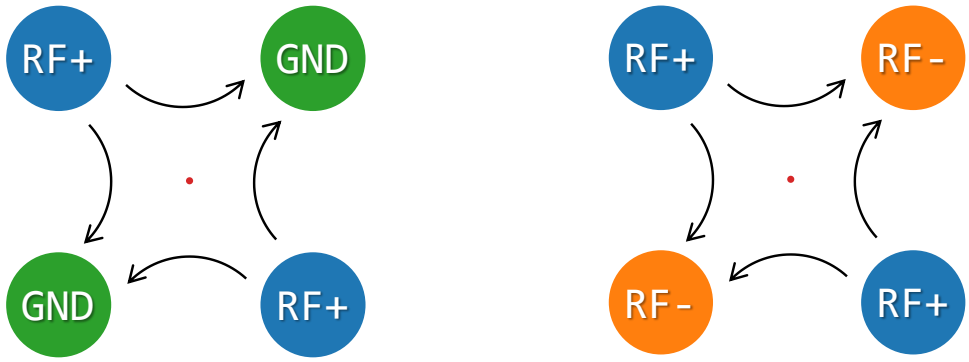

(a) Single RF

(b) Dual RF

Figure 3: Cross section through the four electrodes of a linear Paul trap at one point in time. The trapped ion is represented by the central red dot. The force lines are only qualitative, but indicate that the quadrupole potential is the same for both configurations.

The radial confinement in a linear Paul trap is produced by four straight electrodes in parallel to each other. In the plane perpendicular to the trap axis, the cross section through the rods forms a rectangle. The trapping potential discussed in section 2.1 is created by applying a RF voltage to these rods. Most commonly, two diagonal electrodes are connected to the same RF drive while the two others are connected to ground [6]. The result is qualitatively illustrated in Fig. 3a. An alternative incorporating two different RF signals is shown in Fig. 3b. The two voltages are denoted "RF+" and "RF-" since they are out of phase.

For the Molecules experiment, such a dual RF configuration is chosen and the reasons why are briefly outlined here.

The end goal of the Molecules experiment is to perform high precision spectroscopy on the molecular H_2^+ ions. To this end, the AC Zeeman shift, AC Stark shift and second order Doppler shift in the energy levels have to be small.

For quantum logic spectroscopy experiments, a beryllium ion and ionized hydrogen molecule are simultaneously trapped. Because of this, both ions can not be at the RF zero point at the same time and excess micromotion (denoted by χ in the treatment of the pseudopotential in section 2.1) for at least one of the ions is inevitable. This is were employing a dual RF configuration is advantageous over single RF: For the same RF voltage amplitude, the radial ion confinement is stronger than in the single RF case. Therefore, a smaller RF voltage amplitude is sufficient. This results in a curvature along the trap axis that is smaller, in turn leading to less excess axial micromotion for an ion sitting away from the RF null point. The doppler shift is lowered in this way.

To trap H_2^+ ions with a radial trap frequency of $\sim 7\,\mathrm{MHz}$ in the Paul trap used in the experiment, simulations show that a RF signal of frequency between $45 - 55\,\mathrm{MHz}$ and zero to peak amplitude of $24\,\mathrm{V}$ is required.

3.2 Lumped Component Resonators

This section briefly summarizes the reasons why a resonator comprised of lumped elements is chosen over other common resonator types like helical resonators. A general comparison between different RF resonators can be found in [3] and an overview of helical resonators specifically in [6].

Lumped element circuits offer the flexibility needed to fulfill all of the requirements listed in the previous section. Most importantly, realizing a dual RF drive (see Fig. 3b) is straight forward. Apart from this advantage, they can be designed and ordered as printed circuit boards (PCBs). This allows for a compact design and the addition of functionality and other modifications in a comparatively simple way. Additionally, their behavior can be easily simulated on a computer, which in turn drives the design process.

3.3 Single and Dual RF Resonator Comparison

This section highlights the differences between a basic series RLC resonator circuit as discussed in section 2.2 and the new "dual RF resonator" design. The dual RF resonator consists of two RLC resonators, connected by a shared central capacitance (here: the ion trap). Throughout this report, the two RLC circuits are called the "two sides" of the resonator. The RF signals on the different sides are driven by a single $50\,\Omega$ RF source and share the same frequency, but are relatively shifted in phase by 180°.

The simulations performed here serve the purpose of getting a first estimate of the voltage gain expected when a dual instead of a single RF resonator is used as the drive for an ion trap. The capacitance in the circuits is given by the ion trap rods and identical to the one explained in section 4.1 and seen in Fig. 8b. Here, the more compact denominations

$$C_{\mathrm{TrapGP}} = C_{\mathrm{TrapGP1}} + C_{\mathrm{TrapGP2}} = 18\,\mathrm{pF} \tag{17}$$

for the capacitance of the plus ("P") side to ground ("G") and

$$C_{\mathrm{Trap}} = C_{\mathrm{Trap1}} + C_{\mathrm{Trap2}} + C_{\mathrm{Trap3}} + C_{\mathrm{Trap4}} = 12\,\mathrm{pF} \tag{18}$$

for the trap capacitance between neighboring electrodes are used and the capacitance between diagonal ("D") electrodes C_{TrapD} is neglected. Similarly, the series resistance $R_1 = 0.86\,\Omega$ chosen for the simulations is the sum of a realistic inductor coil's resistance and the trap's measured resistance. The voltage amplitude at the source is chosen to be $V = 2\,\mathrm{V}$. For a $50\,\Omega$ source impedance matched to a $50\,\Omega$ circuit, this corresponds to a voltage of $V = 1\,\mathrm{V}$ at the resonator circuit since the voltage source itself acts as a voltage divider.

For the following analysis, impedance matching (see section 4.4) is implemented with a balun since this leaves the resonant frequency unaffected and equal to the one of a resonator driven by a $0\,\Omega$ ideal source (see section 2.2.1).

All simulations are performed in LTspice [7].

3.3.1 Basic Single RF Circuit

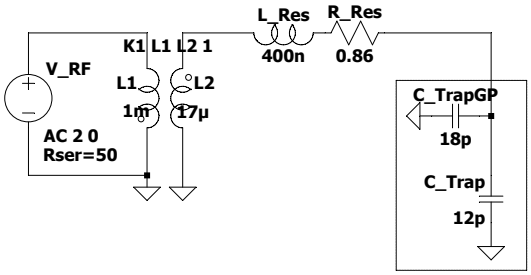

(a) Schematic of the circuit. Impedance matching is achieved with a balun and not discussed here. The trap capacitance is boxed.

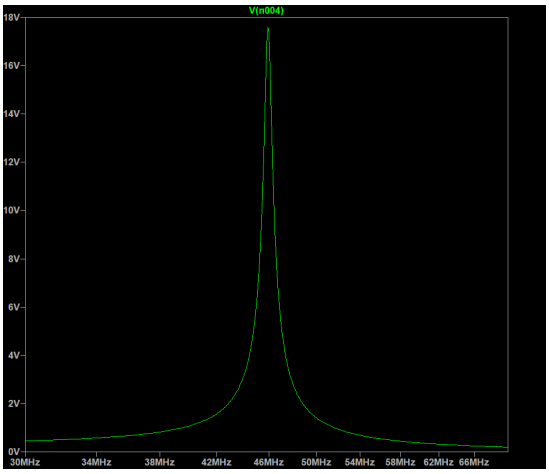

(b) Voltage amplitude over the trap capacitance as a function of frequency. Resonance occurs at approximately 46 MHz and a voltage amplitude of 17.6 V.

Figure 4: Basic series RLC resonator, which is the subject of section 2.2.

For an impedance matched series RLC circuit (see Fig. 4a), the maximal voltage gain G_V is given by equation (16). Inserting the numerical values yields

$$G_V^{\mathrm{m}} = \sqrt{\frac{L}{Z_s RC}} = \sqrt{\frac{400\,\mathrm{nH}}{50\,\Omega \cdot 0.86\,\Omega \cdot (12\,\mathrm{pF} + 18\,\mathrm{pF})}} \approx 17.6, \tag{19}$$

which is in agreement with the simulated value of the peak seen in Fig. 4b.

3.3.2 Basic Dual RF Circuit

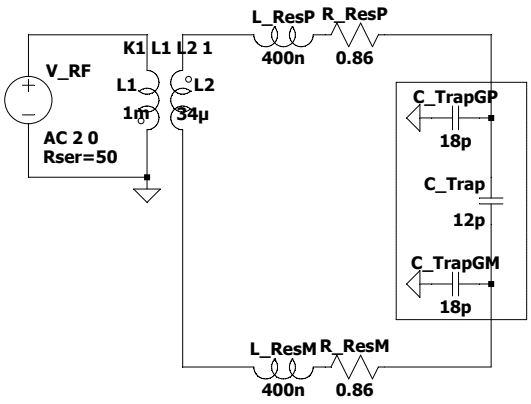

(a) Schematic of a dual RF resonator consisting of two series RLC resonators connected by a central capacitance C_{Trap}. The components ending in "P" and "M" respectively make up what is referred to as the "plus" (top) and "minus" (bottom) side of the circuit.

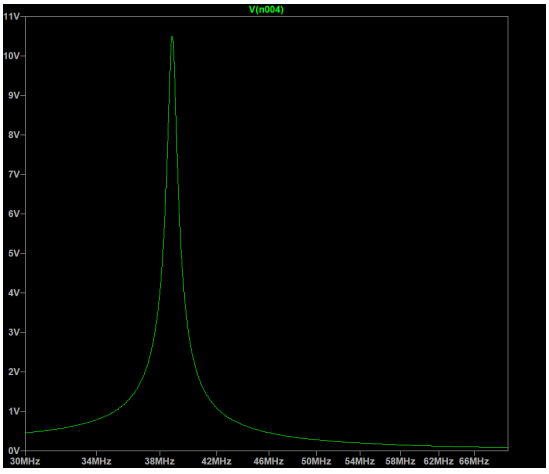

(b) Voltage amplitude over the trap capacitance as a function of frequency. Resonance occurs at approximately 39 MHz and a voltage amplitude of 10.6 V.

Figure 5: Basic dual RF resonator circuit.

The dual RF resonator consists of two single RF resonators (contrast Figs. 4a and 5a), where identical components are added in a symmetrical fashion.

Compared to the single RF case examined in the previous section 3.3.1, the resonance frequency of the dual RF resonator is lowered, while the maximal voltage gain is also reduced. Both changes in the circuit's behavior can be seen when comparing the voltage amplitude over C_{Trap} in Figs. 4b and 5b respectively, where its dependence on frequency is plotted.

Since the resonance frequency can always be easily tuned by changing the resonator coil inductance, the lower voltage gain is of primary concern. From the perspective of the plus side, the reduction in gain can be intuitively explained by interpreting the lower two capacitances C_{Trap} and C_{TrapGM} as a capacitive voltage divider (see section 4.7). Through the capacitive divider, the plus side sees a share of the minus sides's voltage. Since the RF voltage on the two sides has a phase difference of 180°, the magnitude of their complex sum is simply the difference in amplitudes. A calculation yields

$$V_{\text{Dual}} = V_{\text{Single}} \left(1 - \frac{C_{\text{Trap}}}{C_{\text{Trap}} + C_{\text{GrapGM}}}\right) = 17.6\,\text{V} \left(1 - \frac{12\,\text{pF}}{12\,\text{pF} + 18\,\text{pF}}\right) \approx 10.6\,\text{V}, \qquad (20)$$

where the result that the maximal voltage amplitude for a single side is $V_{\text{Single}} = 17.6\,\text{V}$ from equation (19) and equation (24) for a capacitive divider are used.

This result is in very good agreement with the height of the peak in Fig. 5b. Note that when

looking at the circuit in this intuitive way, C_{Trap} is interpreted to act as a part of the single RLC resonator and voltage divider simultaneously.

3.3.3 Hybrid RF Circuit

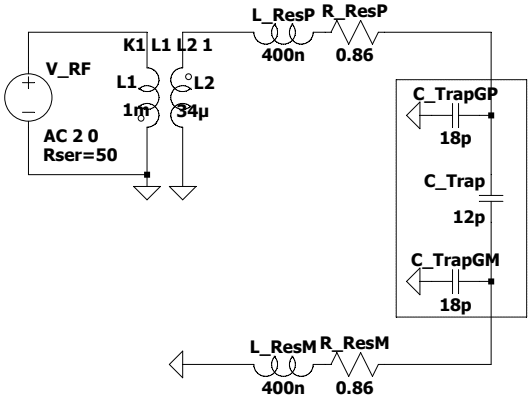

(a) Schematic of the circuit which results from connecting the bottom side of the circuit depicted in Fig. 5a to ground.

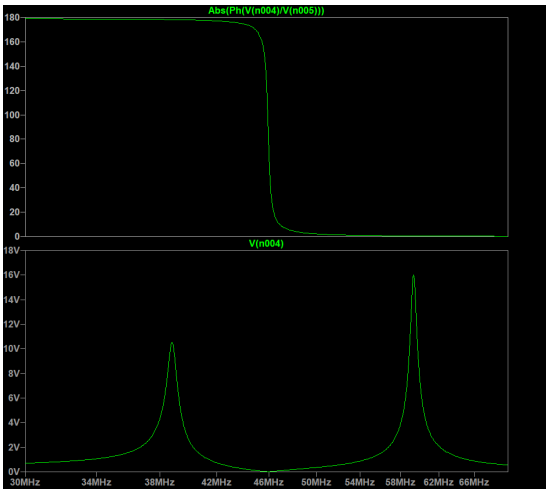

(b) Phase difference between the two sides of the resonator (upper panel) and voltage over the trap capacitance (lower panel) as functions of frequency. The resonances are at approximately 39 MHz (10.6 V) and 59 MHz (15.9 V).

Figure 6: Hybrid between the circuits seen in Figs. 4 and 5.

A hybrid of the resonator circuits discussed in the previous two sections is depicted in Fig. 6a. When comparing this circuit to Fig. 5a, the resonator's minus side is disconnected from the balun and grounded instead.

The frequency dependence of the voltage amplitude over the trap capacitance C_{TrapGP} is plotted in Fig. 6b. There are two resonances visible for this circuit. The resonance at approximately 38.8 MHz is identical to the basic dual RF resonator (see Fig. 5b) and the simulation shows that the two sides have a phase difference of 180° at this frequency. The situation is therefore the same: The two sides act as two out of phase RLC resonators that are connected by a capacitive divider lowering the peak voltage. At a frequency of 59.3 MHz, there appears a second resonance of higher voltage. The circuit's behavior is then analogous to the peak encountered in Fig. 4b, albeit at a different frequency: The voltages on both sides of C_{Trap} are in phase, identical to the single RF case. Because of the larger series resistance, the height of the peak is slightly lower than $V_{\mathrm{Single}} = 17.6\,\mathrm{V}$ seen for that circuit, but larger than in the dual out of phase RF case.

The peak at 38.8 MHz presents an interesting alternative way in which a dual RF resonator can be realized. Instead of externally creating the 180° phase difference with a balun, it arises inherently from a circuit solely consisting of inductances and capacitances. This is potentially useful if the phase shift created by the balun is too imprecise or its loss too high.

4 Dual RF Resonator Circuit

This section is the main part of the report and concerned with the design of a lumped component circuit that fulfills all of the criteria summarized in section 3.1. It is a type of resonator that is referred to as "dual RF resonator" throughout this report, since it consists of two sides denoted "RF+" and "RF-", which have a constant phase difference of 180°. Each of the sides in turn consists of two arms connected to the four electrodes of the ion trap. The final result of the considerations is the schematic included as Fig. 7. A basic version of the dual RF resonator circuit is the subject of section 3.3.2 and included as Fig. 5a. The words "complete" or "full" are used to differentiate the circuit discussed here from that circuit.

The discussion is divided into the sub-circuits making up the complete circuit. They each each serve a particular purpose. Subsection 4.1 is about the capacitance given by the ion trap and section 4.2 treats the inductance forming the resonator together with the trap. Other sub-circuits provide additional functionality: Subsection 4.3 is about how the phase shift between the two arms is created, subsection 4.4 treats impedance matching between the circuit and the RF voltage source, subsection 4.5 how irregularities in the trap capacitance can be compensated and subsection 4.6 is about how a DC bias is applied to the trap rods. Finally, the last two subsections 4.7 and 4.8 present ways in which the amplitude and phase of the RF voltage inside the resonator can be measured during operation.

The values for the idealized components in the simulations are all chosen to ultimately serve the purpose of fulfilling the requirements listed in section 3.1. All of the choices made here reflect the state of knowledge prior to any physical experiments, on the basis of simulations only. Because of this, some alterations to the circuit are anticipated (see outlook in section 6).

The concrete choice of component for every constituent of the circuit can be found in Table 3 in the Appendix and the subsections titled "Component Selection" briefly explain the reasons for the choice.

All of the simulations are conducted in LTspice. An explanation of the commands used can be found as Table 2 in the Appendix.

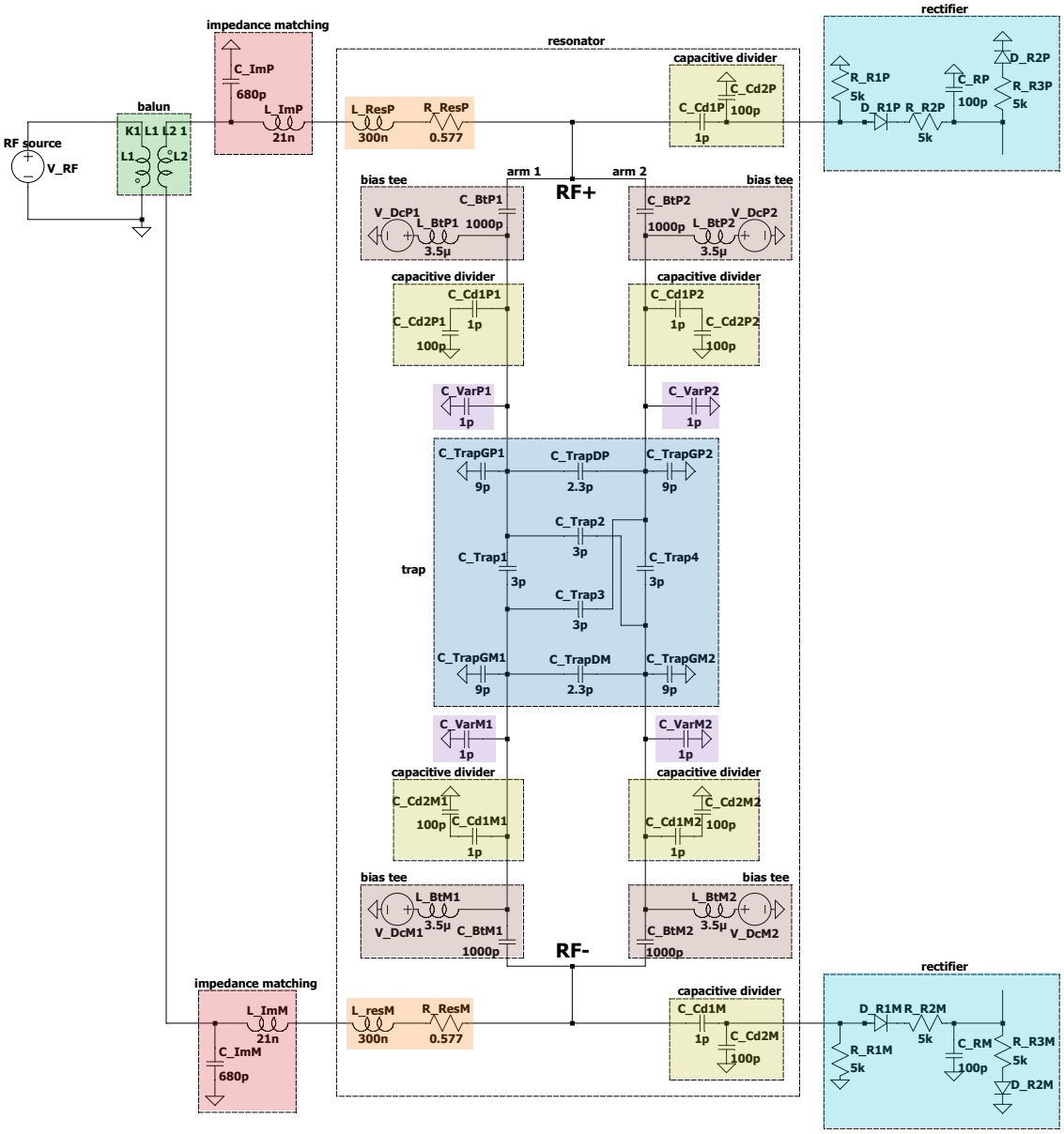

Figure 7: Schematic of the complete dual RF resonator. This circuit serves as the basis for the PCB design and component selection. It is made up of the various sub-circuits in colored boxes, which are discussed separately in the following subsections. The component naming scheme is: {type of component}_{name of sub-circuit}{part of the RF plus (P) or minus (M) side}{optional: part of the 1 or 2 arm}.

4.1 Trap Capacitance

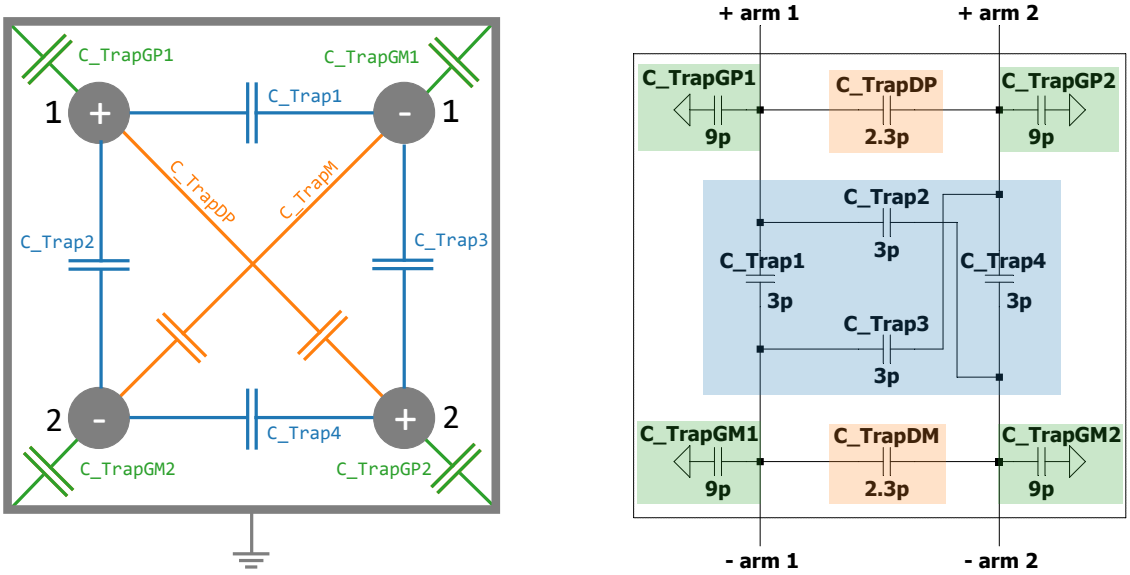

(a) Cross section through the ion trap electrodes to showcase where the capacitances are located and by which scheme they are named.

(b) Detail view of the trap capacitance circuit model used in the simulations.

Figure 8: Geometric and schematic ion trap capacitance model. The colors have no meaning beyond this figure.

The capacitance dominating the oscillation process is given by the ion trap itself. In this section, the model of the trap capacitance used in the simulations is motivated.

A simplified account of the ion trap geometry is illustrated in Fig. 8a in gray: Four metallic rods arranged in parallel form a quadratic cross section and are surrounded by a conducting enclosure. As the laws of electrodynamics predict, there exists a capacitance between all of these conductors. The capacitances between a rod and the ground defined by the housing are drawn in green, capacitances between nearest neighbor rods in blue and capacitances between diagonal rods in orange. The rest of the naming scheme of the rods follows from where they are connected to the dual RF resonator circuit: There are two sides denoted plus and minus that each have two arms termed one and two.

The translation of these trap capacitances into a schematic can be found in Fig. 8b, where the naming and colors are the same as in Fig. 8a. This model of the ion trap capacitance can be used to simulate the resonator circuit and is included in the complete dual RF resonator schematic depicted in Fig. 7.

The numerical values chosen for the model, namely $C_{\mathrm{Trap}\{1,2,3,4\}} = 3\,\mathrm{pF}$ between neighbors, $C_{\mathrm{TrapD}\{\mathrm{P,M}\}} = 2.3\,\mathrm{pF}$ for the diagonal and $C_{\mathrm{TrapG}\{\mathrm{P,M}\}\{1,2\}} = 9\,\mathrm{pF}$ between the electrodes and chamber, are estimated from the measurement results documented in Table 1. Comparing the two, one expects the real capacitances to differ from the model on the order of one pF. The

approximate values are chosen for the model since the uncertainty of the measurements is unknown and the simulation understood to only be an estimate. Since the resonance frequency of the circuit is dependent on the trap capacitances, the resonance frequency found in the real experiment is expected to differ from the simulation. In that case, the resonance frequency can be tuned to the desired value by altering L_{Res} (see sections 4.2 and 6).

Relative Position	**Electrode 1**	**Electrode 2**	**Capacitance [pF]**
nearest			
	top right	bottom right	2.9
	top left	top right	2.9
	bottom left	top left	2.7
	bottom left	bottom right	3.4
diagonal			
	top left	bottom right	2.3
	bottom left	top right	2.7
chamber			
	top right	chamber	8.8
	bottom right	chamber	10.5
	top left	chamber	8.5
	bottom left	chamber	9.3

Table 1: LCR meter measurement results at $f = 1\,\mathrm{kHz}$. The resonator circuit is operated around $f = 50\,\mathrm{MHz}$ and it is unknown how the capacitances differ then.

4.2 Resonator Coil

The resonator coils $L_{\mathrm{Res}\{\mathrm{P,M}\}}$ on the different resonator sides contribute the wanted, non-parasitic inductance to the circuit in the same way the trap model discussed in the previous section 4.1 contributes the primary capacitance. Since the latter is fixed, L_{Res} is the knob to adjust the circuit's resonance frequency. The resonance frequency can always be determined and tuned by simulating the circuit depicted in Fig. 7 in LTspice.

4.2.1 Component Selection

The inductance value is chosen to yield the desired resonance frequency. As an additional consideration, a real inductor coil always has a parasitic series resistance. A higher equivalent series resistance (ESR) inside the resonator leads to higher dissipation, which results in a lower overall Q (see definition (10)) of the circuit. The maximal voltage gain is thus diminished with increasing ESR. The component selected for L_{Res} is therefore chosen to have a low ESR, which is equivalent to it having a large Q_L on its own (see equation (13)). Because of their smaller loss, this criterion is best fulfilled by inductor coils which have an air as opposed to a ceramic core. The comparative downside of air core inductor coils is that for the same inductance, they have a larger footprint than ceramic core ones due to the lower dielectric constant. However, this is not of concern for the application at hand. A tool to find the highest Q inductor coil at a specified inductance and available for purchase from the manufacturer Coilcraft can be found in [8].

4.3 Balun

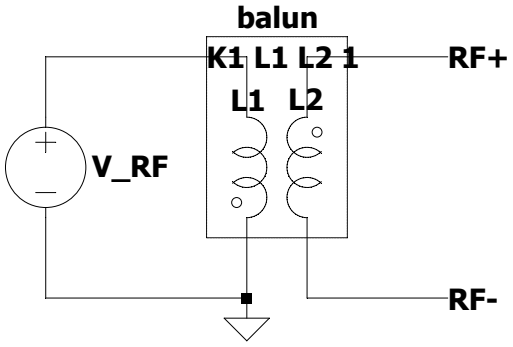

(a) Schematic of a balun consisting of two coupled inductor coils connecting an RF source to the sides "RF+" and "RF-" that ideally have a phase difference of 180°.

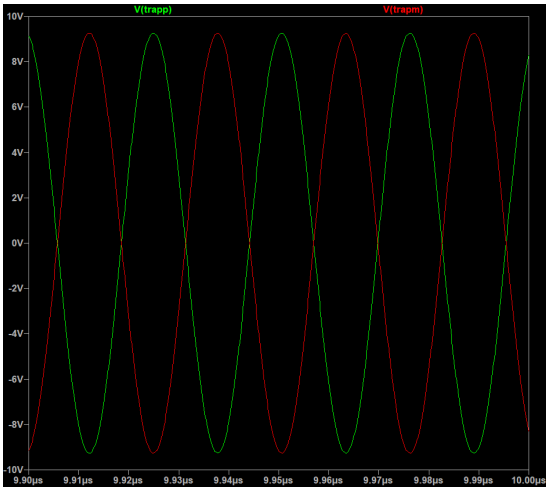

(b) Voltage over C_{TrapGP} and C_{TrapGM} in the basic dual RF resonator circuit (see Fig. 5a) illustrating the 180° phase difference between the resonator's "plus" (plotted in green) and "minus" (plotted in red) side. A 0.1 µs interval interval in the resonator's steady state is chosen.

Figure 9: Balun schematic and phase difference example.

A phase shift of 180° between the dual RF resonator's sides is central to its operation and the reason why they are denoted "RF+" and "RF-" in the first place. This section examines how this phase difference can be created.

The component used to produce the two out of phase RF signals is a transformer, which in this case is called "balun" since it connects an unbalanced line (the RF source) to a balanced line (the resonator circuit). Using a balun in this way allows for the use of a single RF voltage source to drive both the plus and minus side of the resonator. This is desirable since using a single source instead of two ensures that the resonator sides are always driven by precisely the same frequency and have a stable phase relation solely dictated by the balun and trap capacities. The resonator in reference [9] makes identical use of a balun. Reference [10] presents an alternative approach where resonators driven by separate RF sources are coupled by transformers to ensure a constant phase relationship.

4.3.1 Component Selection

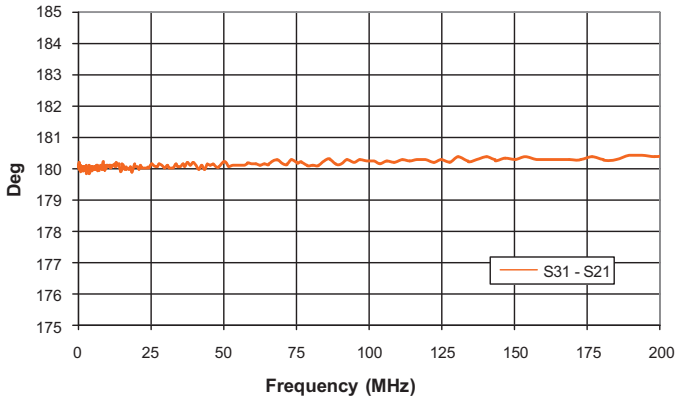

Figure 10: Phase balance as a function of frequency for the component RFXF2513 by MiniRF. The plot is taken from the datasheet provided by the manufacturer [11]. At $f = 50\,\mathrm{MHz}$, the phase shift from 180° is less than 0.3°.

For a real balun component, the phase shift between the two ends is a non constant function of frequency and not always precisely equal to 180° (see Fig. 10). For the dual RF resonator, the main criterion when choosing a balun is therefore a phase shift as close to 180° as possible inside the relevant frequency region.

The balun is chosen with a generic turns ratio of one to one because the largest selection of components is available at this ratio. The turns ratio can be selected arbitrarily because the balun is not used for impedance matching (see section 4.4.2), which is implemented with an L-circuit (see section 4.4.3) instead.

4.4 Impedance Matching

This section gives an overview of so called "impedance matching" between the impedance of the source of the RF signal $Z_s = 50\,\Omega$ and the impedance of the resonator circuit Z_l (generally $\neq 50\,\Omega$). Proper impedance matching is necessary to get the maximal voltage gain possible (see section 2.2.2). The resonator's behavior is illustrated in the unmatched, balun matched and L-circuit matched case. For simplicity, this is done by looking at a RLC resonator circuit, but the results can be adopted to the full resonator depicted in Fig. 7.

4.4.1 Unmatched RLC Circuit

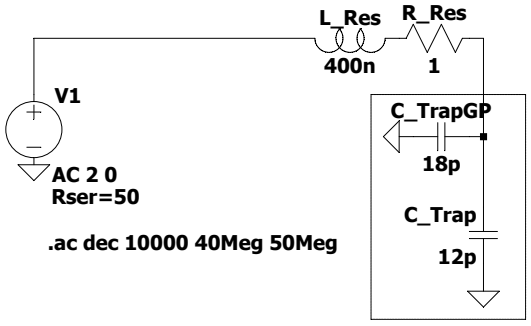

(a) Schematic of a circuit consisting of a series RLC resonator and AC voltage source of impedance $Z_s = 50\,\Omega$.

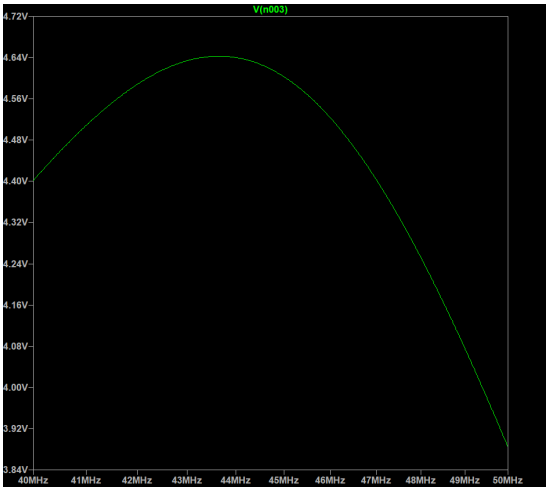

(b) Voltage over the trap capacitance as a function of frequency. Even at resonance, voltage gain is low compared to the impedance matched cases seen in Figs. 12b and 13b.

Figure 11: RLC resonator circuit without impedance matching.

When a non ideal voltage source with a finite impedance $Z_s = 50\,\Omega$ is directly connected to an RLC circuit where no special care to match the load impedance Z_l has been taken, a large fraction of the source's power is back reflected instead of entering the resonator circuit. The result is the low voltage gain and broad frequency response shown in Fig. 11b.

4.4.2 Balun Matched RLC Circuit

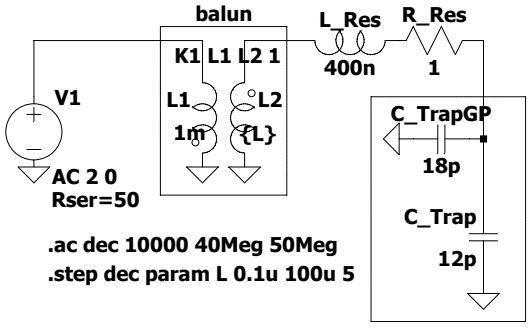

(a) Schematic of the balun impedance matching between a simple series RLC resonator and a $50\,\Omega$ source. The parameter sweep is performed around the resistance ratio of $50\,\Omega/1\,\Omega$, which by equation (21) yields $L_2 = 20\,\mu\text{H}$ if $L_1 = 1\,\text{mH}$ is arbitrarily chosen.

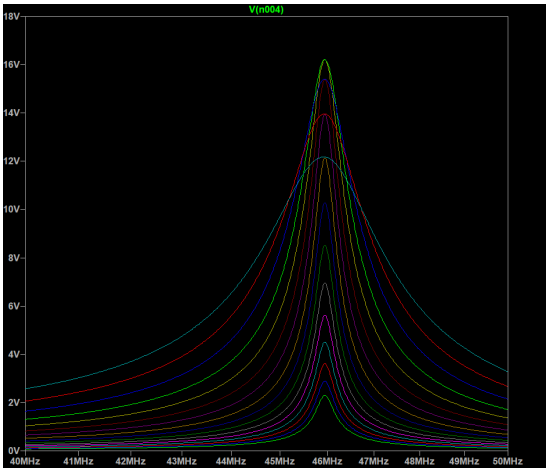

(b) Voltage over the trap capacitance for the circuit and parameter sweep over $\{L\}$ in Fig. 12a. The resonance frequency of the total circuit stays precisely the same while only the amplitude of the resonance varies.

Figure 12: RLC resonator circuit where impedance matching is implemented with a balun.

With a balun, impedance matching can be implemented using the equation from reference [12]

$$\text{turns ratio} = \sqrt{\text{inductance ratio}} = \sqrt{\frac{L_1}{L_2}} = \sqrt{\frac{\text{source resistance}}{\text{load resistance}}}, \tag{21}$$

where it is used that the inductance is quadratic in the number of turns for a standard cylindrical coil inductor and L_1 and L_2 make up the balun as in Fig. 12a.

This is the simplest form of impedance matching since it is completely determined by a single parameter, the turns ratio (or equivalently inductance ratio). Furthermore, for a series RLC circuit, the resonance frequency is unaffected and the voltage gain at resonance is quite stable for small deviations from the optimal value: There is less than a 10% difference in the resonant voltage amplitude for a 50% deviation from the optimal value of L_2. The result of a parameter sweep over L_2 differing by three orders of magnitude is plotted in Fig. 12b.

4.4.3 L-Circuit Matched RLC Circuit

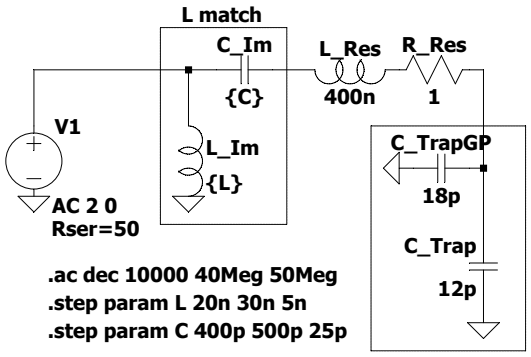

(a) Schematic of the L-circuit impedance matching between a simple series RLC resonator and a $50\,\Omega$ source. The parameter sweep is performed around the calculated optimal values $L_{\mathrm{Im}} = 23\,\mathrm{nH}$ and $C_{\mathrm{Im}} = 464\,\mathrm{pF}$.

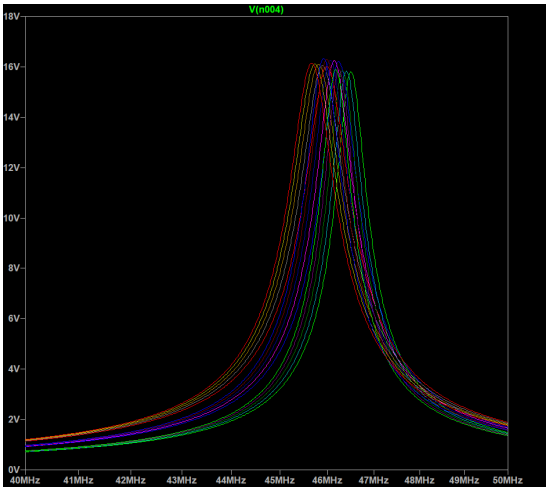

(b) Voltage over the trap capacitance for the circuit and two parameter sweeps over $\{L\}$ and $\{C\}$ in Fig. 13a. One sees that for the different values L_{Im} and C_{Im}, the resonance frequency shifts by less than a MHz, while the peak amplitude stays constant.

Figure 13: RLC resonator circuit where impedance matching is implemented with an L-circuit.

The impedances can also be matched by a so called "L-circuit", of which only one variation is examined here. Alternative implementations can be found in [3].

The load impedance $Z_l = R_l + iX_l$ of the series RLC resonator drawn in the right hand side half of Fig. 13a is easily found by summing $Z_l = Z_{\mathrm{inductor}} + Z_{\mathrm{capacitor}} + Z_{\mathrm{resistor}}$. Since the imaginary part of the impedance has to vanish at resonance (see equation (14)) and resonance is the frequency of interest, only $Z_{\mathrm{resistor}} = 1\,\Omega$ remains, yielding the results $R_l = 1\,\Omega$ and $X_l = 0\,\Omega$. From this, the L-match topology and numerical values at which the load impedance is matched to the source's $Z_s = 50\,\Omega$ can be found [13].

The implementation of impedance matching in this way can be seen in Fig. 13a. A parameter sweep over deviations less than 25% away from the optimal values yields the voltage gain graphs plotted in Fig. 13b. One sees that unlike for the impedance matching with a balun discussed in the previous section 4.4.2, the RLC circuit's resonance frequency is slightly affected by variations in the impedance matching circuit since the additional C_{Im} and L_{Im} contribute capacitance and inductance in addition to L_{Res} and C_{Trap}. For the sweep performed here, the resonance frequency is shifted around inside a 1 MHz interval.

In a harder to track case where the load impedance Z_l can't be easily calculated, Z_l can be determined by simulation. This is the case for the full dual RF resonator schematic in Fig. 7. The load impedance Z_l as a function of frequency is plotted in Fig. 14, where the real and imaginary component can be easily read off for the frequency at which resonance occurs.

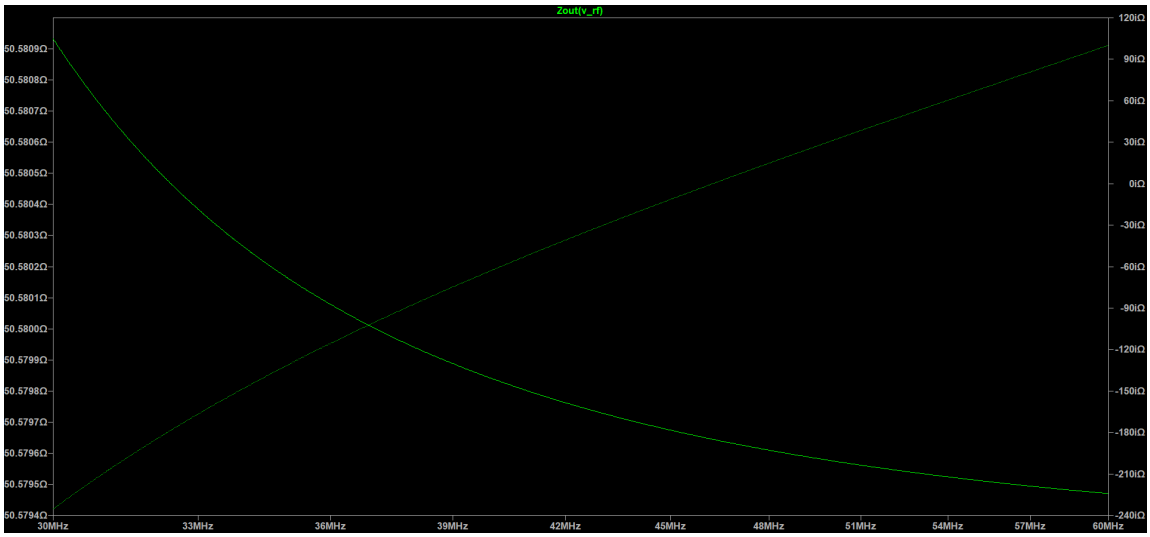

Figure 14: Simulated real and imaginary part of the total impedance Z_l of the full resonator circuit (see Fig. 7) as a function of frequency. The thicker green line plots $\mathrm{Re}(Z_\mathrm{l})$ and belongs to the left hand y-axis, while the thinner green line plots $\mathrm{Im}(Z_\mathrm{l})$ and is associated with the right hand side y-axis.

4.4.4 Component Selection

As the previous subsections show, proper impedance matching is crucial to get the highest possible voltage gain out of a resonator. The first question when it comes to the selection of components for the task is then whether a balun or L-circuit should be used. Using a balun to match the impedances has the considerable disadvantage that only a comparatively small number of different turns ratios are commercially available. In contrast, a large number of different inductor coils and capacitors can be bought. As a result, L-matching circuits can be implemented more flexibly. The choice for the complete dual RF resonator is therefore an L-matching circuit, which is included in Fig. 7.

The capacitor C_Im is chosen for its capacitance value and standard footprint of 0805. The main consideration for the inductor coil L_Im is its inductance and Q value. A large Q is beneficial since it corresponds to a low ESR, and this resistance is detrimental to the resonator circuit's maximal voltage gain. Simulations of the circuit depicted in Fig. 7 show that for the chosen coil, the ESR of L_Im leads to a reduction of the peak voltage by roughly 3%.

4.5 Tunable Capacitors

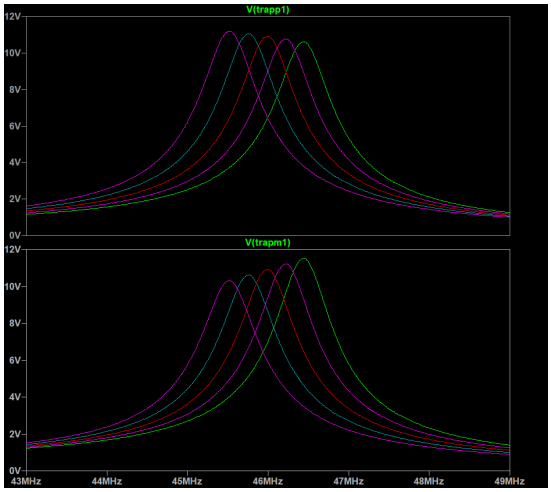

(a) The two panels correspond to the voltage over $C_{\mathrm{TrapG\{P1,\ M1\}}}$. The voltages at arm 2 of the resonator are identical. The red graph corresponds to the assumed model value $C_{\mathrm{TrapGP1}} = 9\,\mathrm{pF}$. Then, the capacitance is arranged completely symmetrically and the two graphs coincide.

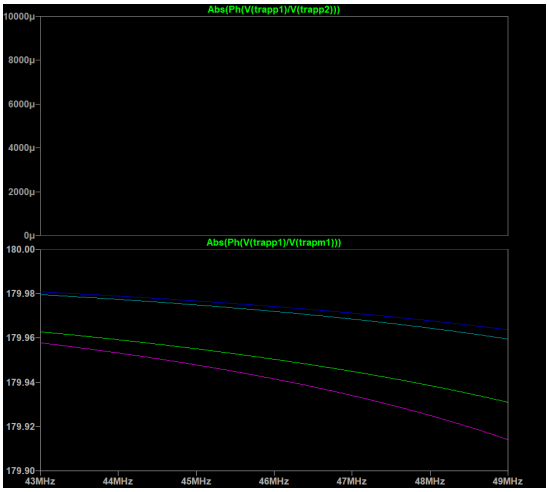

(b) Phase differences between the trap locations denoted P1 and P2 (upper panel) and P1 and M1 (lower panel). The graphs for the other combinations of P1, M1, P2 and M2 are found to be identical: The sweep introduces no phase difference between arms of the same side and an equal phase difference between the sides irrespective of the arm. For the symmetric model value $C_{\mathrm{TrapGP1}} = 9\,\mathrm{pF}$ (red), the phase difference is always equal to 180°.

Figure 15: Voltage and phase difference as a function of frequency simulated for the dual RF resonator circuit depicted in Fig. 7. The graphs of different color are produced by a parameter sweep through $C_{\mathrm{TrapGP1}} \in \{7, 8, 9, 10, 11\}$ pF.

As mentioned in section 4.1 on the ion trap capacitance model, deviations from the assumed trap capacitances shown in Fig. 8b are expected for the real experiment. This section looks into how that potential issue can be compensated.

The parameter sweep plotted in Fig. 15a shows that the resonance frequency changes on the order of MHz when a single one of the capacitances (C_{TrapGP1} in this case) of the trap model is varied in steps of one pF. The particular step size is chosen since it is in line with the expected deviations. The effect of the same sweep on the phase difference between different resonator sides and arms is included as Fig. 15b.

These observations motivate the addition of four variable capacitors $C_{\mathrm{Var\{1,2,3,4\}}}$ to the circuit. They are placed in parallel to the $C_{\mathrm{TrapG\{P1,P2,M1,M2\}}}$, which means that these capacitances add onto each other. This allows one to compensate discrepancies between the actual $C_{\mathrm{TrapG\{P1,P2,M1,M2\}}}$ and their model value. Deviations in the $C_{\mathrm{Trap\{1,2,3,4\}}}$, which also have an influence on both the resonant frequency and phase, can not be compensated this way.

4.5.1 Component Selection

The premier consideration when choosing a tunable capacitor component is their range. Since it is measured that $C_{\mathrm{TrapG}} \approx 9\,\mathrm{pF}$, capacitors with $C_{\mathrm{Var}} = 1 - 5\,\mathrm{pF}$, which is smaller but of the same order, are chosen. In addition, these capacitors are manually adjustable with a screwdriver and offer a comparatively stable value.

4.6 Bias Tee

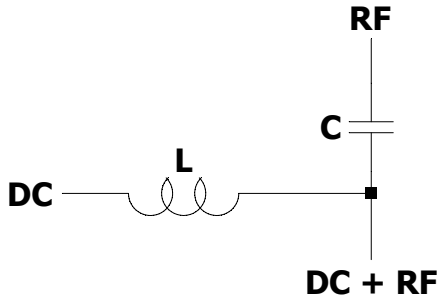

Figure 16: Schematic of a bias tee consisting of a capacitor C and inductor L.

The resonator circuit has to be able to provide separate static DC potentials to the individual electrodes of the trap. This section looks at how this is implemented.

A bias tee allows one to combine a static (DC) and an alternating (RF) voltage in the arrangement illustrated in Fig. 16. In the practical setting of the ion trap, the wire denoted "RF" is provided by a RF resonator circuit and "DC" is supplied by a separate voltage source. Then, "DC+RF" is the voltage at which one of the trap's rods (see Fig. 8a) sits. A bias tee is employed to serve the same function in the resonator circuit devised in reference [10].

For the bias tee to operate in its correct regime where the RF and DC voltages are separated in the sense that the RF component at the position denoted "DC" is negligible and vice versa, the following two relations have to be fulfilled [14]

$$X_C = \frac{1}{\omega C} \ll Z \tag{22}$$

$$X_L = \omega L \gg Z \tag{23}$$

In these equations, Z is the impedance of the connected transmission line, X_C the solely complex impedance of the idealized capacitor and X_L the likewise complex impedance of the inductor. Under these conditions, C can be intuitively interpreted as an ideal capacitor allowing all RF to pass while blocking all DC and L as an ideal inductor blocking all RF while allowing all DC to pass.

By allowing the existence and control of the DC bias, the bias tee additionally serves as a DC/GND reference. This makes sure that no charge accumulates on the trap's rods.

4.6.1 Component Selection

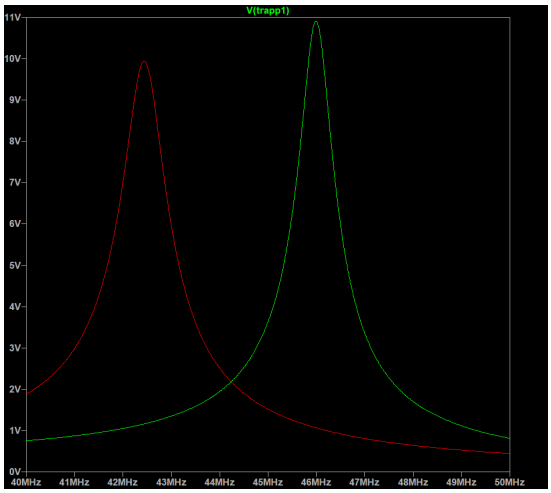

(a) Voltage amplitude over the trap capacitance C_{TrapGP1} as a function of frequency with (green graph) and without (red graph) the four bias tees. The graphs show that the inclusion of bias tees influences the resonance and they have to be taken into account in the simulations. The difference in amplitude is due to the impedance matching not being adjusted to the case without bias tees.

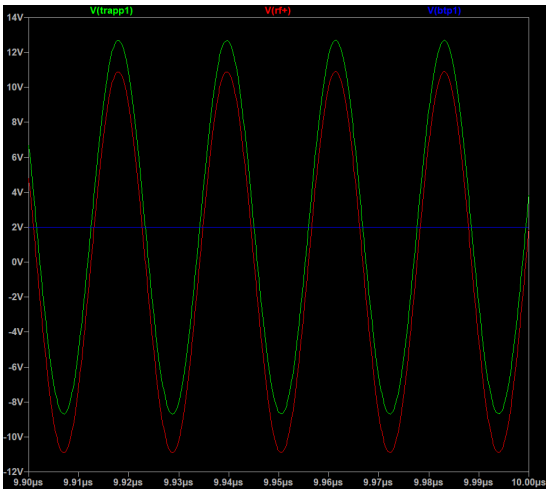

(b) Transient analysis showing a 0.1 µs interval when the resonator is in a steady state. The voltage over the trap capacitance C_{TrapGP1} is plotted in green, the potential at the RF+ location in red and the DC bias in blue. Green is observed to be the sum of red and blue.

Figure 17: Simulation results of the complete dual RF resonator circuit from Fig. 7.

The full circuit drawn in Fig. 7 employs a total of four bias tees where the wires denoted "DC" are connected to one DAC each.

The result of a simulation comparing the resonator circuit's behavior with and without the four bias tees are plotted in Fig. 17a. One can see that their inclusion does have a non negligible influence on the resonance frequency. This is acceptable because the unwanted resonance frequency shift can be anticipated with the simulation and L_{Res} adjusted to yield the correct overall resonance frequency. The graphs in Fig. 17b show that the chosen components C_{Bt} and L_{Bt} fulfill the conditions in equations (22) and (23): The RF, DC and RF+DC outputs are separated from each other.

Analogous to the situation described in sections 4.2.1 and 4.4.4, a low ESR for both C_{Bt} and L_{Bt} is desirable for maximal voltage gain. Simulating the circuit drawn in Fig. 7 with $V_{\mathrm{RF}} = 2\,\mathrm{V}$ shows that for the chosen components, the ESR of the real capacitor C_{Bt} leads to a reduction in voltage gain by approximately 2%. Similarly, the ESR of the real inductor L_{Bt} reduces the voltage gain by roughly 10%. One additional observation from the simulations is that the larger L_{Bt}, the less its ESR matters for the maximal voltage gain.

4.7 Capacitive Divider

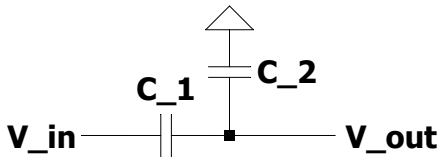

Figure 18: Schematic of a capacitive divider consisting of two capacitors C_1 and C_2.

The aim is to measure the full RF signal comprised of amplitude and phase at the rods forming the trap without disturbing the resonance.

The capacitive divider discussed here serves the purpose of protecting the dual RF resonator circuit from the influence measurement with a probe has on its operation. The basic schematic is illustrated in Fig. 18. For such a layout, the following equation holds

$$V_{\text{out}} = \frac{C_1}{C_1 + C_2} \cdot V_{\text{in}} \,, \tag{24}$$

where V_{in} and V_{out} are the amplitudes of the RF voltage. A capacitive divider only passes negligible parasitic DC input, which is ideal since only the RF is of interest here.

For the dual RF resonator circuit in Fig. 7, $C_1 \ll C_2$ is chosen. Then, the influence a $50\,\Omega$ oscilloscope measurement has on the resonance is negligible, if it is performed behind the capacitive divider [15]. The resulting low output voltage $V_{\text{out}} \ll V_{\text{in}}$ is not problematic because voltage measurement with a connected oscilloscope is very sensitive.

In total, four capacitive dividers with $50\,\Omega$ SMA connectors at V_{out} are placed for this purpose, one for each ion trap rod. Two additional capacitive dividers are placed in front of the rectifier sub-circuits (see section 4.8) for similar reasons.

4.7.1 Component Selection

Simulations show that a ratio of $C_2/C_1 = 100$ yields the desired behavior where the circuit is only insignificantly disturbed and V_{out} still measurable. The capacitance $C_1 = 1\,\text{pF}$ is chosen to be as small as possible and determines $C_2 = 100\,\text{pF}$. The components chosen have a standard footprint of 0805.

4.8 Rectifier

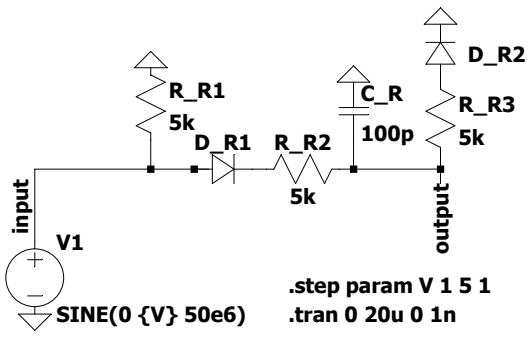

(a) Schematic of the rectifier sub-circuit incorporated on each side of the dual RF resonator circuit in Fig. 7. There, it is placed behind a capacitive divider.

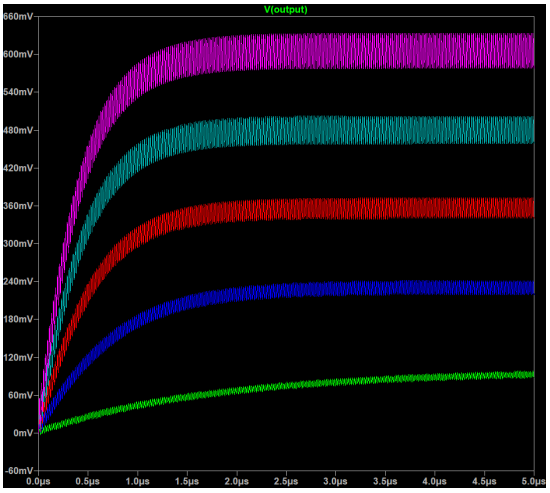

(b) Voltage measured at the location denoted "output" in Fig. 19a. For the sweep of the parameter $\{V\}$, the lowest graph (green) corresponds to $V = 1\,\mathrm{V}$ and the uppermost graph (violet) to $V = 5\,\mathrm{V}$ with steps of $1\,\mathrm{V}$ between them.

Figure 19: Rectifier sub-circuit schematic and simulation.

The rectifier sub-circuit outlined in this section serves a diagnostic purpose similar to that of the oscilloscope measurement discussed in the previous section 4.7. The difference is that in this case not the full RF signal, but only its maximal amplitude is of interest. That way, a simple DC measurement can be performed with a multimeter and there is no need for an oscilloscope.

In the full dual RF resonator circuit depicted in Fig. 7, there is one rectifier per side. It is placed behind a capacitive divider, which is done to ensure that the rectifier only has negligible influence on the resonator circuit itself.

The schematic of the rectifier can be found in Fig. 19a and the time response of the output voltage in Fig. 19b. One sees that the lower the input voltage, the longer it takes until equilibrium is reached. This does not constitute a problem for the purposes of the resonator circuit since that time interval is short in comparison to the measurement timescale. One can also see from the simulation that the equilibrium DC output voltage increases approximately linearly with respect to the amplitude of the input RF voltage if it is sufficiently large. The conversion factor in the range between $0.5\,\mathrm{V}$ and $1\,\mathrm{V}$ (which corresponds to an RF amplitude of approximately $50\,\mathrm{V}$ to $100\,\mathrm{V}$ before the capacitive divider) can be found to be

$$V_{\mathrm{out}} \approx 0.1292 \cdot V_{\mathrm{in}} - 0.0350\,\mathrm{V} \tag{25}$$

by simulating the circuit in LTspice. The result is included as Fig. 20. This relationship can be experimentally verified by comparing the DC measurement at the rectifier with the oscilloscope measurement discussed in section 4.7.

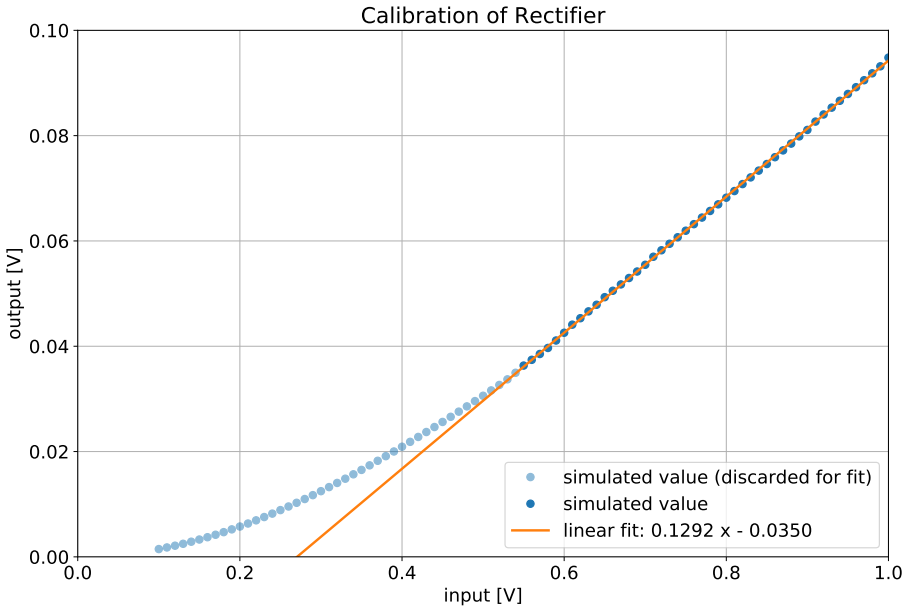

Figure 20: The blue dots are the equilibrium output voltages of the rectifier, which are determined as the average of the last thousand data points in simulations such as the ones plotted in Fig. 19b. The linear fit plotted in orange is calculated only considering input voltages greater than 0.5 V (darker blue dots). For smaller input voltages, the output voltage is found to change non linearly (lighter blue dots).

4.8.1 Component Selection

The components used here are chosen because they were previously used in a similar single RF resonator circuit designed for the IntIon experiment (see semester thesis [16]).

5 PCB Design

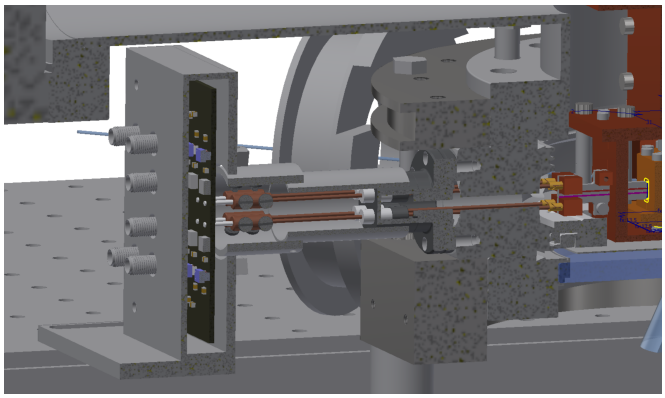

Figure 21: 3D model of the final PCB attached to the chamber in which the ion trap is located.

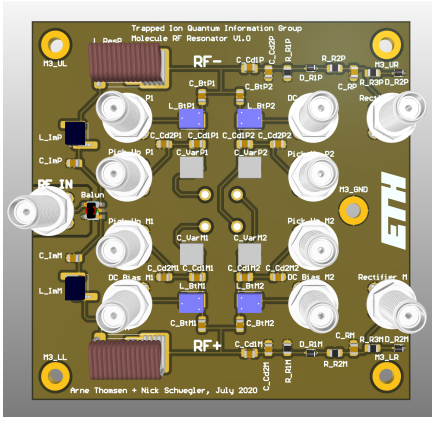

Figure 22: Overhead view of the 3d model of the PCB.

This section briefly describes how the dual RF resonator circuit devised in section 4 and illustrated in Fig. 7 is translated into a printed circuit board (PCB) design.

5.1 Symmetry

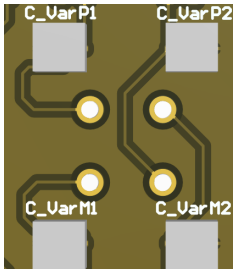

Figure 23: Detail view of the central region of Figure 22. The routing leading to the trap electrode connectors can not be made completely symmetric because of the differing relative rod positions in the schematic (see Fig. 8b) and actual ion trap (see Fig. 8a). The routing is designed to yield identical path lengths in spite of this.

When operating the dual RF resonator, a phase difference of precisely 180° between the two sides denoted "RF+" and "RF-" is essential. Section 4.3 describes how this originates at the balun. In that discussion and the simulations conducted in LTspice, the dependence of the RF voltage's phase on path length is neglected. For a real circuit, this simplification does not hold and careful consideration has to be put into the physical routing on the PCB.

The simplest way to ensure that the half wavelength phase difference at the balun is preserved at the connection to the ion trap rods is to have a completely symmetrical design with respect to the two resonator sides. The path lengths between the balun and the connector rods of a single arm are then guaranteed to be identical on both sides. Additionally, the path length between the balun and the two rods of a single side have to be identical as well, which is not automatically given: When comparing Figs. 8a and 8b in section 4.1 on trap capacitance, one sees that rods on the same resonator side are diagonal to each other inside the ion trap, but next to each other on the schematic. This asymmetry is accounted for by the routing seen in Fig. 23.

The above ensures equal path lengths on the PCB itself, but not at the connection to the ion trap (see sections 5.2 and 6).

5.2 Input/Output

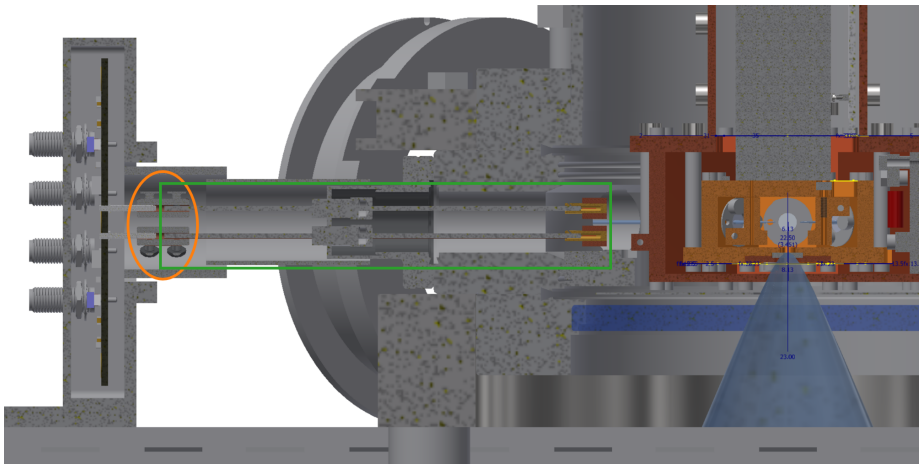

Figure 24: Perpendicular view of the PCB attached to the ion trap. Encircled in orange are the ion trap rods (left), PCB rods (right) and the barrel connector that links them. Boxed in green is the part of the assembly seen in Figure 25.

Some of the sub-circuits of section 4 require an input or output to either some type of voltage source or measuring device. For this reason, a total of 11 standard SMA connectors are placed on the PCB: 1 for the RF voltage source, 4 to apply a DC voltage to the bias tees, 4 for pick up at the capacitive dividers and 2 for pick up at the rectifiers.

Additionally, the PCB has to be connected to the ion trap. The four ion trap electrodes exit the vacuum chamber as four rods arranged in a square (see Fig. 21). To ensure that the phase difference between the RF signals inside the ion trap is correct, the path length between the four PCB rods and the ion trap rods has to be identical. These are the same considerations as in section 5.1, but external to instead of on the PCB.

Identical path lengths are achieved most easily by a connection that is designed around the four rods in a symmetric manner. Therefore, the PCB is placed in the plane perpendicular to the rods, as illustrated in Fig. 21. The connection between the PCB and ion trap rods is realized with a

barrel connector. This leaves room for path length differences, which is an anticipated problem for real life operation of the resonator and briefly discussed in the outlook (section 6).

5.3 Additional Considerations

Additional thoughts put into the design of the PCB are collected in this subsection.

The resonator circuit is sensitive to parasitic capacitances and inductances as they shift around the resonance frequency. For this reason, all of the components are connected on a single PCB layer and no vias are used. This choice also simplifies the symmetry requirements.

The choice of components is discussed in more detail in the "Component Selection" subsections of section 4. As a rough rule, the footprints are chosen to be as general as possible, such that different variants of the components can be soldered onto the PCB without having to redesign it. Therefore, most components are chosen to be of the standardized 0805 size. The inductor coils however are primarily chosen for their high Q and therefore have non standard footprints. For example, they differ in length for different inductances. To accommodate alternative component selection, the footprints are overlaid on the PCB in this case.

There are no stringent requirements for the PCB size as it is placed outside the vacuum chamber (see Fig. 21). This makes it straight forward to follow the spacing guidelines required for the safe operation of a high voltage PCB found in reference [17]. The mechanical mounting is realized with screws and the PCB includes four holes to accommodate them.

In section 3.3.3, the behavior of the full dual RF resonator circuit is contrasted with a version where one of the sides is grounded instead of directly connected to the balun. This is called the "hybrid RF resonator" there. As seen in the simulations, the two out of phase RF signals are then realized for a specific frequency range without the need for a balun. Therefore, this modification to the circuit is potentially interesting and the PCB design includes solder bridges to ground that allow for this change to be made.

6 Conclusion and Outlook

The original scope of this semester thesis included testing of the physically realized PCB. This experimental section which would have required presence in the laboratory could not be realized because of restrictions on the work semester students could perform during the spring semester of 2020 due to the global pandemic Covid-19.

In accordance with the situation, the semester project was adjusted. More time was spent on the conception of the circuit with extensive simulations, which are summarized in section 4 and on thoroughly designing the PCB, section 5. Hopefully, this careful preparation work leads to a smaller number of needed iterations of the resonator circuit until it satisfies all requirements in real life, which can never be fully anticipated.

With the design of the underlying circuit and concrete PCB having reached a conclusion, the next steps are ordering and assembling the PCB. As an outlook, two main difficulties are expected to arise afterwards in operation; namely deviations between the modeled and true ion trap capacitance and improper phase difference at the trap electrodes. They are shortly discussed in the following paragraphs.

The model schematic of the ion trap capacitance used in the simulations is outlined in section 4.1 and a photograph of the electrodes forming the real ion trap is included as Fig. 1b in the

Introduction. When looking at the photograph, one can tell that there is an obvious asymmetry between the two visible electrodes: The lower one is right next to the copper housing while the upper one is not. From this observation alone, the capacitance to ground is expected to be different in the two cases. This is neglected in the model. Additionally, there are various potential sources of parasitic capacitance on the path between the electrodes and the rods ultimately connecting to the PCB. These expected imperfections can not be accounted for beforehand, because of the limitations in the capacitance measurement found in Table 1.

When the finished resonator PCB is finally attached to the trap, the capacitance dependent resonance frequency is therefore expected to differ from the value obtained in the simulations. By adjusting the unknown trap capacitance model, the resonance frequency of the known circuit can then be reproduced inside the simulation. With the updated model, the new resonator coil inductance yielding the desired resonance frequency can be found. The coil can then be swapped out on the PCB (see sections 4.2.1 and 5.3) and compared to the simulation. In this way, the desired resonance frequency is achieved step by step.

Information on the resonance frequency is available in the first place by connecting an oscilloscope to one of the 4 diagnostic SMA connectors when the frequency at the RF source is varied.

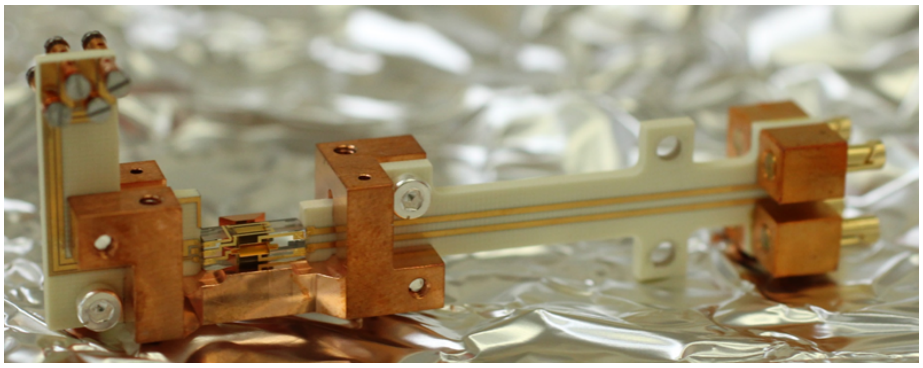

Figure 25: Photograph of the ion trap assembly and connections. This whole construction is inside the vacuum chamber. Fig. 1b shows a closeup view of the trap, which is visible in the left part. The wire bonding between the glass enclosed trap electrodes and connectors is visible there. Likewise, the link between these connectors and four golden ones is visible to the right.

The second anticipated problem is a phase difference between "RF+" and "RF-" at the ion trap electrodes not equal to 180° because of unequal path lengths.

Fig. 25 shows an overview of the ion trap assembly. In the end, the location where the phase difference needs to be correct is at the trap electrodes. One sees that that the connection between the electrodes on the left and the rods leaving the vacuum chamber on the right of the photographs involves multiple different parts. The connections between them (gold wirebonds and components glued together with silver epoxy) are expected to be imperfect, in turn leading to different path lengths. This means that even if all of the path lengths on the PCB are equal and the four connections between the PCB and ion trap are perfect, the final phase difference at the trap electrodes can still be incorrect. For this reason, a separate solution to precisely control the path lengths may have to be designed.

References

[1] *Molecules*. URL: https://tiqi.ethz.ch/research/molecules.html. (accessed: 12.06.2020).

[2] F. Lindenfelser. "Broadband cooling on a forbidden transition in a novel high-optical-access ion trap". PhD thesis. 2017.

[3] D. Gandolfi. *Compact RF Amplifier for Scalable Ion-Trap*. 2011.

[4] Rainer Wallny. "Wellenlehre, Elektrizität und Magnetismus - Skriptum zur Vorlesung Physik II Frühjahrssemester 2017 an der ETH Zürich (unpublished)". 2017.

[5] A.V.Bakshi, U.A.Bakshi, and A.P.Godse. *Network Analysis*. Technical Publications, 2006. ISBN: 9788189411237.

[6] J.D. Siverns et al. "On the application of radio frequency voltages to ion traps via helicalr resonators". In: *Applied Physics B* 107 (2012), pp. 921–934.

[7] *LTSpice*. URL: https://www.analog.com/en/design-center/design-tools-and-calculators/ltspice-simulator.html. (accessed: 03.06.2020).

[8] *Highest Q Finder*. URL: https://www.coilcraft.com/apps/finder/hiqfinder.cfm. (accessed: 03.06.2020).

[9] Da An et al. "Surface trap with dc-tunable ion-electrode distance". In: *Review of Scientific Instruments* 89.9 (2018), p. 093102. DOI: 10.1063/1.5046527. eprint: https://doi.org/10.1063/1.5046527. URL: https://doi.org/10.1063/1.5046527.

[10] Amelia Detti et al. "A compact radiofrequency drive based on interdependent resonant circuits for precise control of ion traps". In: *Review of Scientific Instruments* 90.2 (2019), p. 023201. DOI: 10.1063/1.5063305. eprint: https://doi.org/10.1063/1.5063305. URL: https://doi.org/10.1063/1.5063305.

[11] *Balun Datasheet*. URL: http://www.minirf.com/pdf/transformers/RFXF2513DS.pdf. (accessed: 20.05.2020).

[12] Iulian Rosu. *Impedance Matching*. URL: https://www.qsl.net/va3iul/Impedance_Matching/Impedance_Matching.pdf. (accessed: 19.04.2020).

[13] *RF Impedance Matching Calculator*. URL: https://www.analog.com/en/design-center/interactive-design-tools/rf-impedance-matching-calculator.html. (accessed: 18.04.2020).

[14] *Bias Tee*. URL: https://en.wikipedia.org/wiki/Bias_tee. (accessed: 22.05.2020).

[15] D. Gandolfi et al. "Compact radio-frequency resonator for cryogenic ion traps". In: *Review of Scientific Instruments* 83.8 (2012), p. 084705. DOI: 10.1063/1.4737889. eprint: https://doi.org/10.1063/1.4737889. URL: https://doi.org/10.1063/1.4737889.

[16] K. Reuer. *Radio Frequency Voltage Sampling at Cryogenic Temperatures*. 2017.

[17] Lazar Rozenblat. *CALCULATING SPACING BETWEEN PCB TRACES FOR VARIOUS VOLTAGE LEVELS*. URL: https://www.smps.us/pcbtracespacing.html. (accessed: 15.05.2020).

A Appendix

A.1 Spice Commands

Spice Command	**Explanation**
.step param ⟨X⟩ ⟨X0⟩ ⟨X1⟩ ⟨Xstep⟩	The variable X is linearly incremented from the starting value X0 to the final value X1 in steps of size Xstep. The units don't have to be specified and all automatically correspond to the physical quantity X is associated with.
.ac dec ⟨S⟩ ⟨F0⟩ ⟨F1⟩	AC frequency analysis on a decadic logarithm range where F0 and F1 specify the minimal and maximal frequency and S is the number of simulation points per power of ten.
.tran ⟨Tprint⟩ ⟨Tstop⟩ ⟨Tstart⟩ ⟨Tmaxstep⟩	Transient analysis in time, where the circuit's state is simulated for every time step. Tstop specifies the final time of the simulation, Tstart the first and Tmaxstep the largest time step allowed between two consecutive simulation points.
SINE(⟨DC⟩ ⟨V⟩ ⟨F⟩)	Sinusoidal AC source voltage, where DC specifies the DC-offset, V the amplitude of the voltage and F the frequency.
⟨K1⟩ ⟨L1⟩ ⟨L2⟩ ⟨k⟩	Create a transformer K1 by coupling two coils L1 and L2. The parameter k is equal to one for an ideal transformer.

Table 2: Explanation of spice commands used in the simulations.

A.2 List of Components

Designator	Value	Manufacturer	Part Number	x
Resonator				
$L_{\mathrm{ResP}}, L_{\mathrm{ResM}}$	300 nH	Coilcraft	2222SQ-301	2
$C_{\mathrm{VarP1}}, C_{\mathrm{VarP2}}$, $C_{\mathrm{VarM1}}, C_{\mathrm{VarM2}}$	1-5 pF	Johanson Manufacturing	2320-1	4
Balun				
Balun	1:1	MiniRF	RFXF2513	1
Impedance Matching				
$C_{\mathrm{ImP}}, C_{\mathrm{ImM}}$	680 pF	Murata	GRM21A5C2E681JWA1	2
$L_{\mathrm{ImP}}, L_{\mathrm{ImM}}$	21 nH	Coilcraft	1812SMS-22N	2
Bias Tee				
$C_{\mathrm{BtP1}}, C_{\mathrm{BtP2}}$, $C_{\mathrm{BtM1}}, C_{\mathrm{BtM2}}$	1 nF	Murata	GRM21A5C2E102JWA1	4
$L_{\mathrm{BtP1}}, L_{\mathrm{BtP2}}$, $L_{\mathrm{BtM1}}, L_{\mathrm{BtM2}}$	3.3 µH	Coilcraft	1812CS-332	4
Capacitive Divider				
C_{Cd1P},C_{Cd1M}, $C_{\mathrm{Cd1P1}}, C_{\mathrm{Cd1P2}}$, $C_{\mathrm{Cd1M1}}, C_{\mathrm{Cd1M2}}$	1 pF	American Technical Ceramics	600F1R0BT250XT	6
$C_{\mathrm{Cd2P}}, C_{\mathrm{Cd2M}}$, $C_{\mathrm{Cd2P1}}, C_{\mathrm{Cd2P2}}$, $C_{\mathrm{Cd2M1}}, C_{\mathrm{Cd2M2}}$	100 pF	Murata	GQM2195C2E101GB12	6
Rectifier				
$R_{\mathrm{R1P}}, R_{\mathrm{R1M}}$, $R_{\mathrm{R2P}}, R_{\mathrm{R2M}}$, $R_{\mathrm{R3P}}, R_{\mathrm{R3M}}$	5.1 kΩ	Vishay Dale	CRCW08055K10FKEA	6
$C_{\mathrm{RP}}, C_{\mathrm{RM}}$	100 pF	Murata	GQM2195C2E101GB12	2
$D_{\mathrm{R1P}}, D_{\mathrm{R1M}}$, $D_{\mathrm{R2P}}, D_{\mathrm{R2M}}$	-	Diodes Incorporated	1N5711WS-7-F	4
Input/Output				
SMA Connector	50 Ω	Amphenol RF	132134	11
Rod	0.05”	Mill-Max	4357-0-00-15-00-00-03-0	4
Barrel Connector	0.05”	Lesker	FTAIBC072	4

Table 3: Components used for the initial design.

A.3 PCB

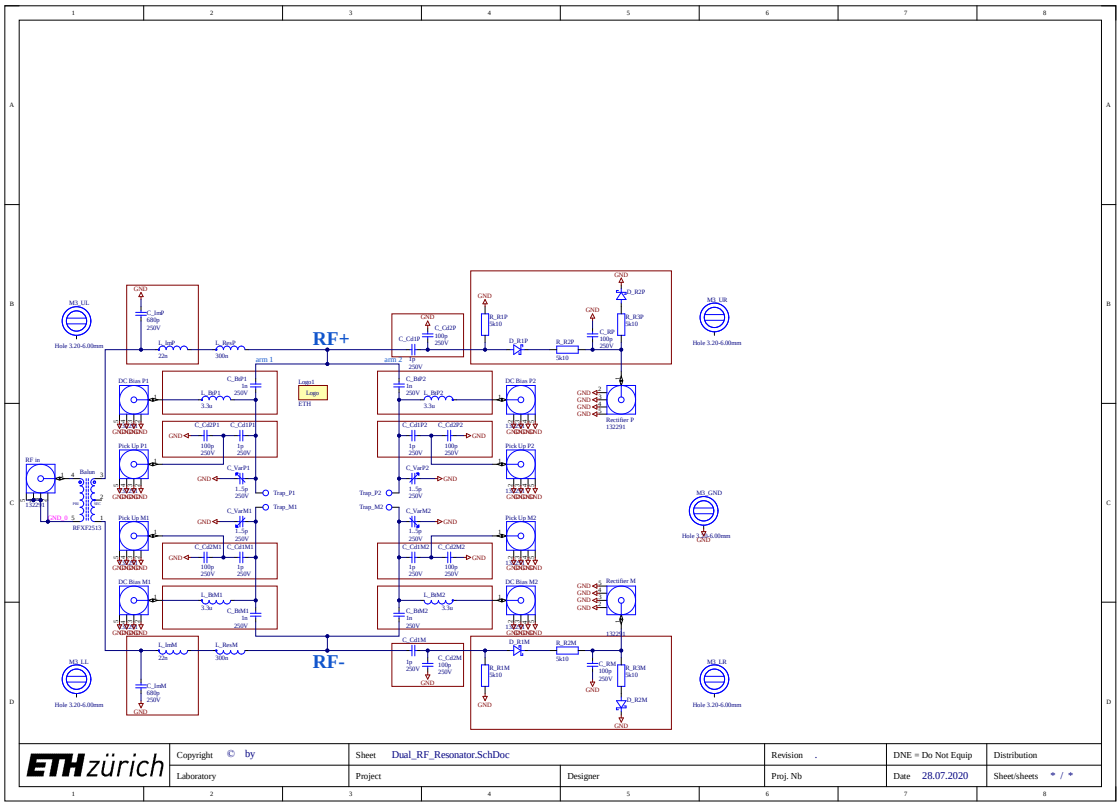

Figure 26: Schematic of the PCB exported from Altium. The basic circuit is identical to Fig. 7 from LTspice, but includes the input/output components while excluding the model of the ion trap capacitance.

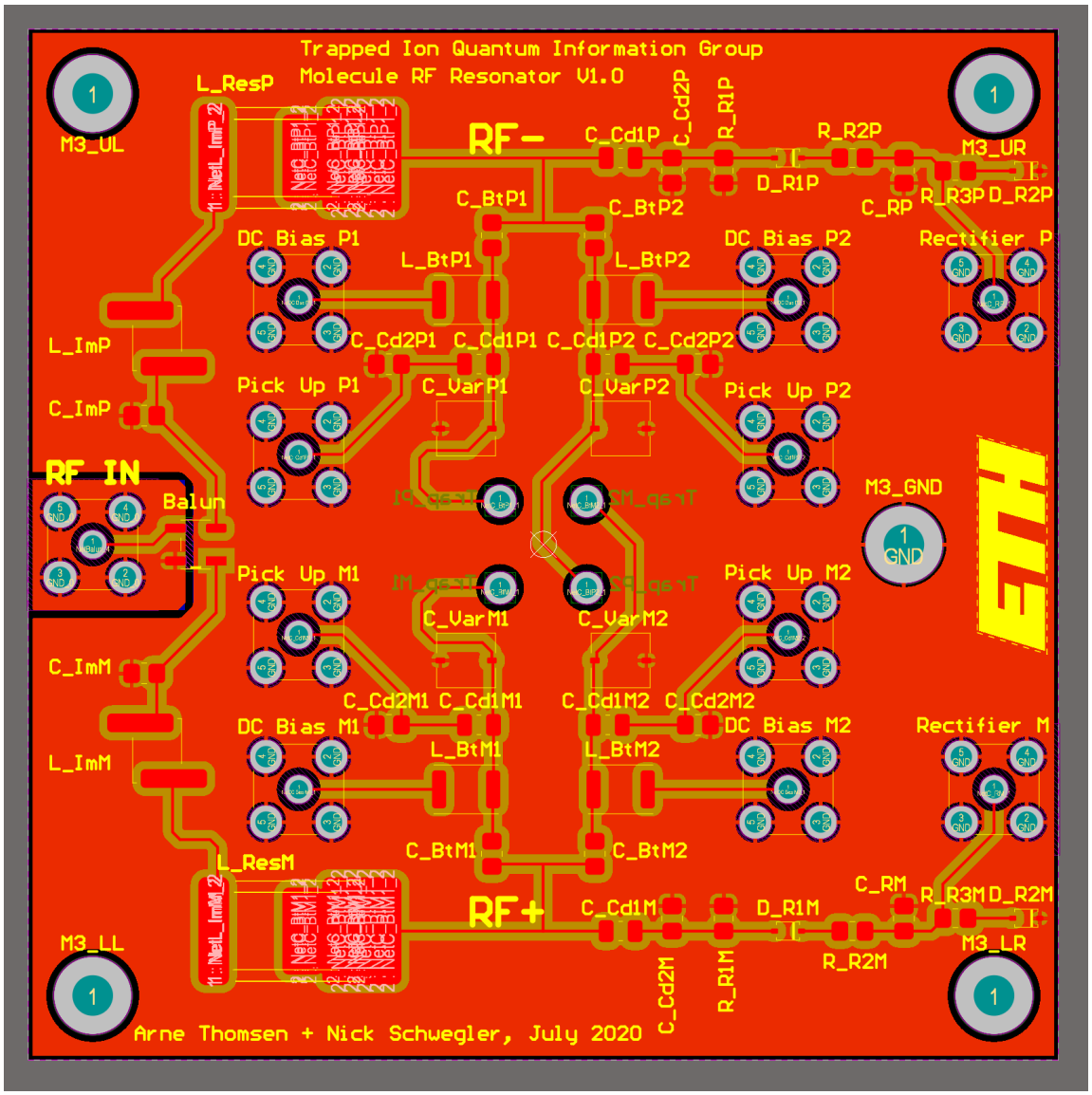

Figure 27: PCB top layer.